Performance evaluation of a transformerless multiphase electric submersible pump system

Ahmed A. Hakeem[1], Ahmed Abbas Elserougi[1], Ayman Samy Abdel-Khalik[1], Shehab Ahmed[2], Ahmed Mohamed Massoud[1,3]

[1]*Department of Electrical Engineering, Alexandria University, Alexandria, Egypt*
[2]*ECEN Department, Texas A&M University at Qatar, Doha, Qatar*
[3]*Electrical Department, Qatar University, Doha, Qatar*
E-mail: ahmed.abbas@spiretronic.com

Published in *The Journal of Engineering*; Received on 11th June 2014; Accepted on 9th July 2014

Abstract: Using of low-voltage variable-frequency drive followed by a step-up transformer is the most preferable way to feed an electrical submersible pump motor. The existence of long feeder between the motor and drive systems usually causes over-voltage problems because of the travelling wave phenomenon, which makes the employment of filter networks on the motor or inverter terminals mandatory. The so-called boost-inverter inherently can solve this problem with filter-less operation as it offers a direct sinusoidal output voltage. As boost inverters have voltage boosting capability, it can provide a transformer-less operation as well. This study investigates the performance of a five-phase modular winding induction machine fed from a boost-inverter through a long feeder. A simulation study using a 1000 Hp system and experimental investigation on a 1 Hp prototype machine are used to support the presented approach.

Nomenclature

V_{dc}	input DC voltage
V	amplitude of the inverter phase voltage
f	fundamental frequency
f_s	switching frequency
R_f	resistance of the feeder per kilometres
L_f	inductance of the feeder per kilometres
C_f	capacitance of the feeder per kilometres
L_i	input inductance
R_i	input resistance (series with each inductor)
C_i	boost-inverter output capacitance
I_L	inductor current
$\hat{v}_c$	peak of the capacitor voltage
$\hat{I}_{Ph}$	peak of the load current
$I_{L\ max}$	peak of the inductor current
Δv_C	capacitor voltage ripple
ΔI_L	inductor current ripple
D	duty cycle of DC–DC converter
R_s	stator resistance per-phase
R_r	rotor resistance per-phase
L_s	stator inductance per-phase
L_r	rotor inductance per-phase
L_m	magnetising inductance per-phase

1 Introduction

Electrical submersible pump (ESP) systems are one of the most important systems in offshore oil platform facilities [1]. In ESP systems, variable-frequency drive (VFD) through a medium voltage long feeder is used to supply the electric power to the ESP motor [2, 3]. An ESP system generally consists of multiple centrifugal pump stages, a submersible electrical motor and an armor-protected long feeder [4]. The motors have long stacks and limited diameters and are generally designed with very special form factors [5, 6]; the winding of such machines is one of the costly and time-consuming manufacturing steps. Owing to their odd form factor, ESP motors are manually wound induction machines. A five-phase modular induction machine alternative was proposed in [7] as a potential means to reduce production time by enabling automated winding of the ESP motor when segmented stators are utilised. The machine architecture also overcomes the limitations of modular winding three-phase induction machines [8]. Moreover, multiphase machines offer additional degrees of freedom that have promoted them as serious contenders in various applications [9].

The distributed LC line impedance and the fast rise/fall time of the inverter voltage lead to a reflected wave phenomenon that causes doubling and ringing of the motor terminal voltage at the long feeder's receiving end (RE) [10, 11]. Furthermore, starting problems because of the voltage drop along the feeder are more significant with high-inertia motor loads [2]. More problems arise, such as bearing currents and electromagnetic interference, because of the high dv/dt of the inverter voltage [12, 13]. To overcome over-voltage problems, the filters are commonly employed. Several topologies have been proposed in the literature to mitigate the effect of long motor leads [10, 13]. Two topologies have commonly emerged; an RC filter at the RE of the long feeder [14], and an RLC filter at the sending end (SE) of the long feeder [15]. In addition to these two topologies, more topologies have been discussed qualitatively in [16–18], where two filter topologies have been developed to reduce the common-mode voltage problem mentioned before [16]. Additionally, an LC resonant filter with a diode bridge may be used, but is limited to low-voltage drives [17]. A common-mode transformer, with a conventional inverter output filter mitigates common-mode currents [18, 19]. An integrated differential-mode and common-mode filter have been presented in [13].

In the field of ESP systems, motors are typically fed from a step-up transformer and a low-voltage VFD based on a classical voltage source inverter (VSI) topology. The so-called boost-inverter [20–22] naturally generates, in a single stage, a boosted sinusoidal output voltage and allows for transformer-less operation with relatively small passive elements instead. Additionally, the above-mentioned problems associated with a VSI are inherently mitigated as the inverter generates a direct sinusoidal voltage output. Hence, feeding a submersible pump motor with a modular induction machine using a five-phase boost-inverter is proposed as a viable new topology with both application and economic benefits. This topology offers potential economic benefits, transformer-less operation and concurrent natural mitigation of long feeder

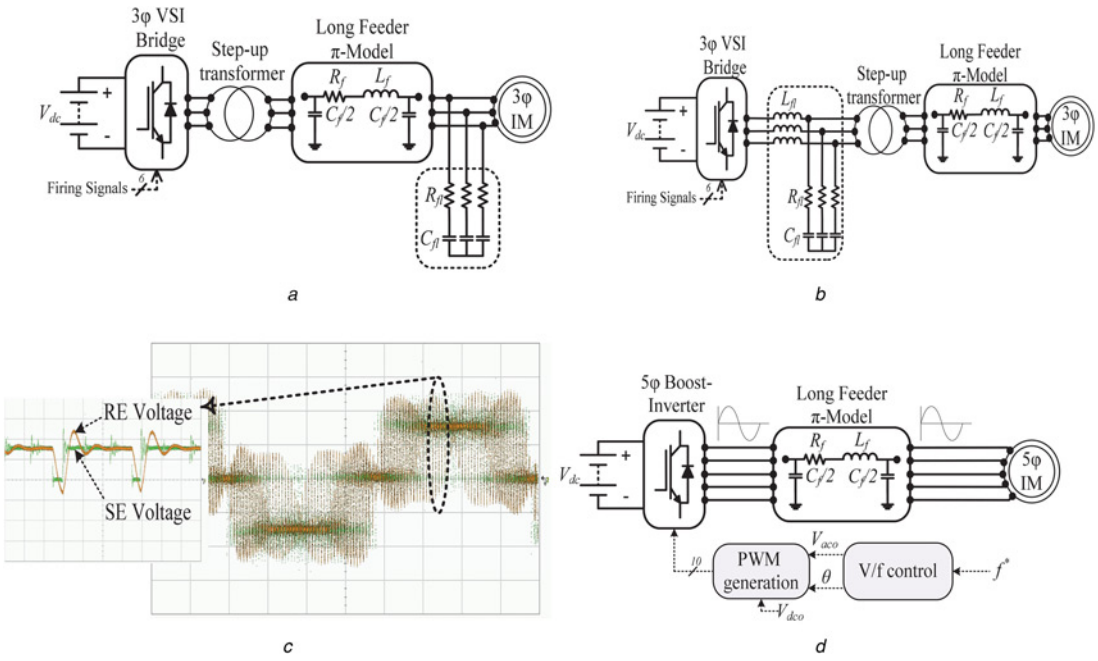

Fig. 1 *Three-phase VFD-ESP system*
a Using RC filter at the long feeder RE
b Using RLC filter at the long feeder SE
c Experimental results of the over-voltage problem because of the long feeder in the VSC-based VFD-ESP system (50 V/div)
d Five-phase boost-inverter-based VFD-ESP system diagram

consequences. A prototype system is built and used for experimental validation using a 1 Hp five-phase modular induction machine, a five-phase boost-inverter and a long feeder emulated using the conventional π-network model.

2 VSI-based VFD-ESP system

A conventional VSI-based VFD-ESP system consists of a low-voltage VFD, a step-up transformer, a downhole cable and an ESP motor. Two filter topologies are generally employed, as shown in Figs. 1*a*, and *b*. The reflected wave phenomenon associated with the presence of the long feeder in the ESP system with the VSI is shown in Fig. 1*c*. This figure shows the RE phase voltage across the prototype motor terminals when fed from a conventional VSI without filters. The machine experiences a notable voltage rise because of the distributed impedance nature of the feeder and the fact that the motor impedance appears as an open circuit relative to the feeder impedance [10].

3 Proposed boost-inverter-based VFD-ESP system

In this section, the proposed ESP system is presented. The general system block diagram is depicted in Fig. 1*d*. In this system, the low-voltage VSI, step-up transformer and the required filter in Figs.1*a*, and *b* are replaced by a boost-inverter, whereas the three-phase induction machine is replaced by a five-phase modular induction machine. The detailed discussion of each part is given in the subsequent sections.

3.1 Five-phase modular induction machine

In [7], a detailed comparative performance and design study between conventional multiphase induction machines with distributed windings and five-phase modular induction machines is carried out. The general conclusions drawn from such a study prove that the modular multiphase induction machine can be a viable alternative to its three-phase counterpart, but with a power density penalty. Fig. 2 shows the stator winding layout of a

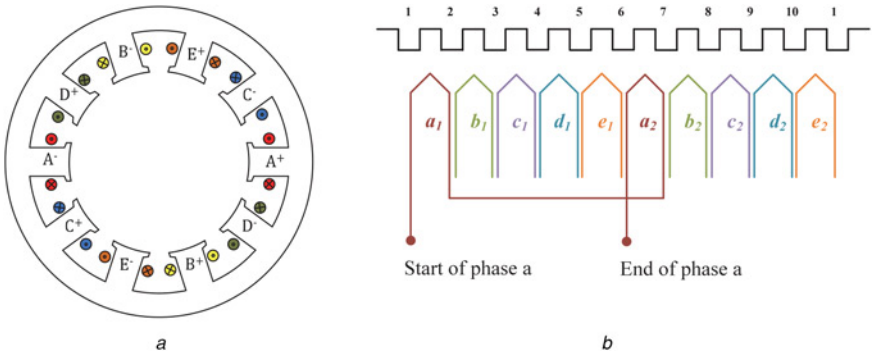

Fig. 2 *Five-phase modular machine stator winding layout*
a Stator layout
b Winding layout

doi: 10.1049/joe.2014.0148

2-pole five-phase modular induction machine. This machine is shown to have the following features [7]:

- The modular construction offers potentially lower winding production cost for long stack, limited diameter applications.
- The additional degrees of freedom because of the higher number of phases offer higher fault tolerant capability.
- For the same power rating and same phase voltage, a five-phase machine draws less line current. Consequently, both cable voltage drop and losses are reduced.
- There are two available operating sequences, namely primary and secondary sequences. The secondary sequence gives a synchronous speed of one third that obtained when the primary sequence is applied, whereas phase current magnitudes corresponding to the primary and secondary sequences are close in value for the same load. In other words, this winding offers two speed operation by only changing the applied voltage sequence.

On the other hand, the main drawback of this machine configuration is that the copper volume used is approximately double that of a conventional three-phase induction machine, thus requiring a slightly higher outer diameter because of the increase in the total slot area to accommodate the increased number of turns.

3.2 *Five-phase boost-inverter*

A single-stage five-phase boost-inverter provides not only DC-to-AC five-phase conversion but also voltage boosting capability, and inherent output filtering. The system consists of five DC–DC bi-directional boost converters sharing the same common point (O) as shown in Fig. 3*a*. The load is connected to phases *a*, *b*, *c*, *d* and *e*. These converters produce a DC-biased sine wave output via controlling the duty cycle (D_j) of each DC–DC converter. The AC component of each converter output is 72° out of phase. The common point of the capacitors is connected to the negative terminal of the DC-link. The five-phase motor is connected to the inverter terminals which is electrically isolated from the capacitors' common point.

In this topology, the output voltage reference of each DC–DC converter is composed of AC and DC components as in (1), where V_{dco} and V_{aco} represent the DC and AC components of the converter output voltage, respectively.

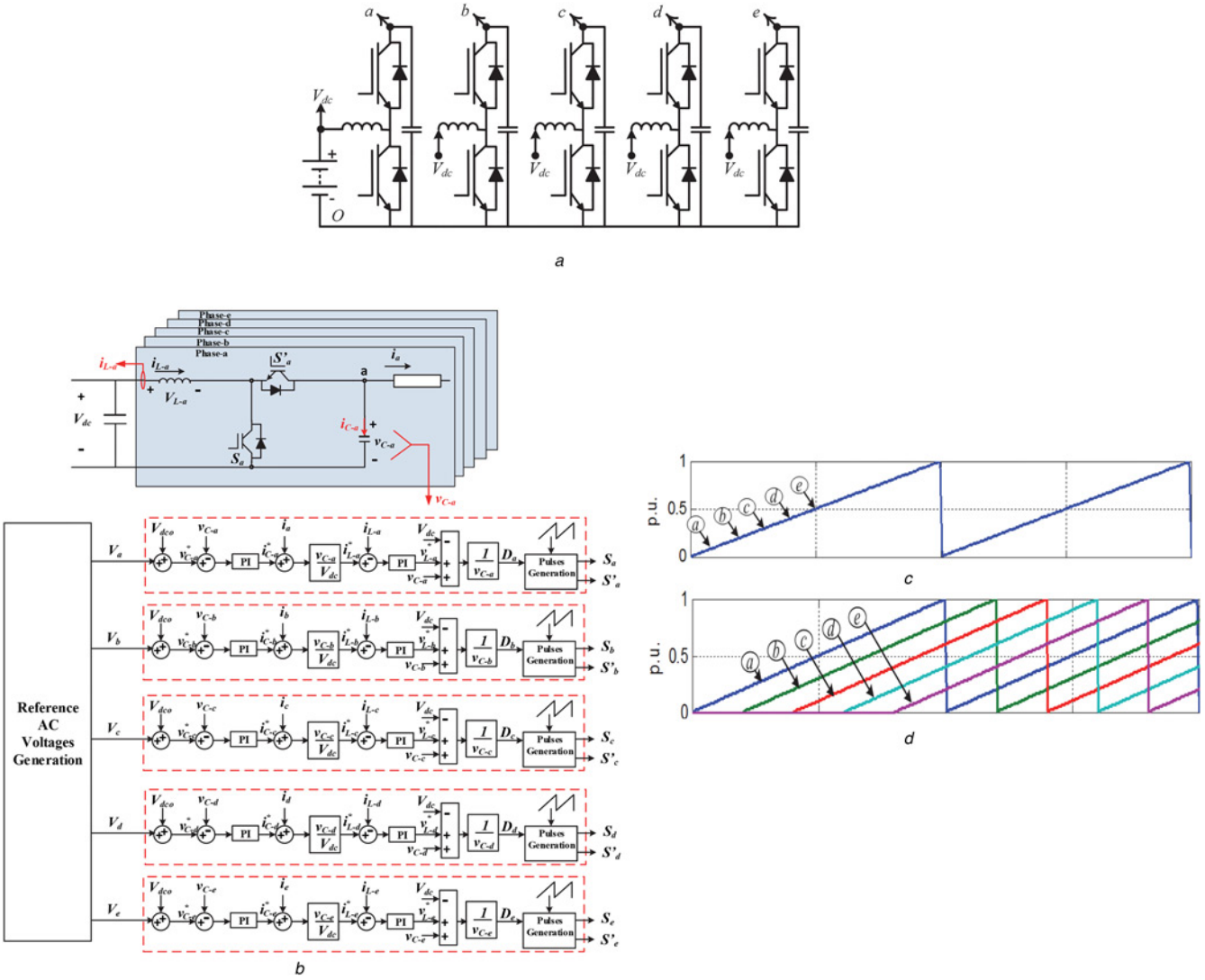

Fig. 3 *Five-phase boost-inverter*
a Topology
b Boost-inverter controller
c Un-shifted carrier of a five-phase boost-inverter
d Shifted carrier of a five-phase boost-inverter

The DC component should be the same for all phases and greater than or equal to the sum of the AC component peak and the DC input voltage (V_{dc}) to avoid operating at zero duty cycle. The AC side terminals are trapped between the capacitors connected to the upper insulated gate bipolar transistors (IGBTs). For equal DC components, the five line voltages are sinusoidal. Equation (2) shows the converter's output line voltage with eradicated DC components.

Each boost DC–DC converter has to be controlled to ensure robust performance during different operating conditions. The closed-loop control schemes for the single-phase boost-inverter are proposed by [20, 21] to ensure robust performance during different operating conditions

$$\begin{aligned} v_{aO}(t) &= V_{\text{dco}} + V_{\text{aco}} \sin(\omega t) \\ v_{bO}(t) &= V_{\text{dco}} + V_{\text{aco}} \sin\left(\omega t - \frac{2\pi}{5}\right) \\ v_{cO}(t) &= V_{\text{dco}} + V_{\text{aco}} \sin\left(\omega t - \frac{4\pi}{5}\right) \\ v_{dO}(t) &= V_{\text{dco}} + V_{\text{aco}} \sin\left(\omega t - \frac{6\pi}{5}\right) \\ v_{eO}(t) &= V_{\text{dco}} + V_{\text{aco}} \sin\left(\omega t - \frac{8\pi}{5}\right) \end{aligned} \tag{1}$$

$$v_{ab}(t) = v_{aO}(t) - v_{bO}(t) = 1.1756\, V_{\text{aco}} \sin\left(\omega t + \frac{3\pi}{10}\right) \tag{2}$$

The double-loop regulation scheme for a five-phase boost-inverter is shown in Fig. 3*b*. The reference voltages are biased by V_{dco}. The DC bias can be obtained by adding the input voltage V_{dc} to the peak output amplitude. The voltages across capacitors $V_{C\text{-}a}$, $V_{C\text{-}b}$, $V_{C\text{-}c}$, $V_{C\text{-}d}$ and $V_{C\text{-}e}$ are controlled to track the voltage references using proportional–integral (PI) controllers. The currents through L_a, L_b, L_c, L_d and L_e are also controlled by PI controllers to achieve stable operation by estimating suitable instantaneous duty cycles for each DC-to-DC converter (D_a, D_b, D_c, D_d and D_e). The duty cycle signals are compared with carrier waveforms to generate gate pulses for the semiconductor devices (IGBTs). It has to be noted that it is better to use shifted carriers (as in Fig. 3*d*) to reduce the inverter DC current ripples.

Selection of boost-inverter parameters (inductors, capacitors and switching frequency) is a very important design consideration. The inductors are designed for continuous operation with certain acceptable inductor current ripple; on the other hand, the capacitors are selected to limit the output voltage ripple. Finally, the switching frequency is selected based on the required converter rating and switch type. The design steps for the boost-inverter parameters are presented in detail in Appendix.

When the machine is operating under *V/f* control, the desired speed is used to determine the suitable input frequency. Then, the machine voltage amplitude is selected to maintain a constant *V/f* ratio.

3.3 Long feeder model

The long feeder can be functionally represented by an equivalent π-network model using lumped constants as shown in Fig. 1. This model is capable of giving acceptable results during both steady state and transient periods [10]. More sophisticated models can improve system modelling as presented in [11].

4 Five-phase boost-inverter-based VFD-ESP system design

Since the target applications for the proposed machine are mainly in the high-power arena, a case study has been conducted for the proposed five-phase boost-inverter-based VFD-ESP system on a 2400 V/1000 Hp five-phase induction machine with the rating and parameters listed in Table 1. The feeder utilised in this case is AWG 1/0 whose parameters are listed in Table 1.

4.1 Boost-inverter design

In this system, the boost-inverter output voltage has to be higher than the machine rated voltage to overcome the voltage drop across the long feeder. At machine full-load current, the voltage drop across the feeder is 30 V_{rms}. Therefore, the root-mean-squared (rms) value of the inverter output voltage must be kept at ~2430 V to guarantee delivery of 2400 V at the machine terminals when operating at a frequency of 60 Hz.

If a DC-link voltage of 2 kV is used, the DC component level must be selected to ensure that

$$V_{\text{dco}} > 2000 + (2430\sqrt{2})$$

that is, the DC component must be >5437 V, so 5500 V is assigned to V_{dco}.

The full parameters and ratings of the boost-inverter are listed in Table 1. The maximum instantaneous value of the duty cycle is shown in (3)

$$D_{\max} = 1 - \left(V_{\text{dc}}/\hat{v}_{\text{c}}\right) = 1 - \left(\frac{V_{\text{dc}}}{V_{\text{dco}} + V_{\text{aco}}}\right) \cong 0.78 \tag{3}$$

From (8), the inductor current peak is ~500 A. Practically, the inductor current ripple is selected to be 20% of the inductor current peak, that is, $\Delta I_{\text{L}} = 100$ A.

The relation between inductor current ripple and its inductance is given by (4)

$$\Delta I_{\text{L}} = \frac{(V_{\text{dc}} - I_{\text{L max}}\, R_{\text{i}}) D_{\max}}{L_{\text{i}} f_s} \cong \frac{1520}{L_{\text{i}} f_{\text{s}}} \tag{4}$$

Table 1 Parameters of high-power simulated case study

	Parameters	Values
five-phase modular machine	number of poles	4
	f, Hz	60
	connection	Y
	rated phase voltage, V rms	2400
	rated power, Hp	1000
	rated phase current, A rms	70
	R_{s}, Ω	0.8755
	X_{s}, Ω	4
	$R_{\text{r}}^{'}$, Ω	0.4116
	$X_{\text{r}}^{'}$, Ω	3.246
	X_{m}, Ω	195.6
	total inertia	40 kg m^2
	friction coefficient	0.5 N m/rad/s
feeder	L_{f}, mH/km	0.296
	R_{f}, Ω/km	0.426
	C_{f}, μF/km	0.3
	feeder length, km	1.0
five-phase boost-inverter	L_{i}, mH	3
	R_{i}, Ω	0.1
	C_{i}, μF	50
	inductor rating, A	600
	capacitor rating, kV	10
	f_{s}, kHz	5
	V_{dco}, V	5500
	V_{aco}, V	$2430\sqrt{2}$
	semiconductor switches rating	600 A, 10 kV

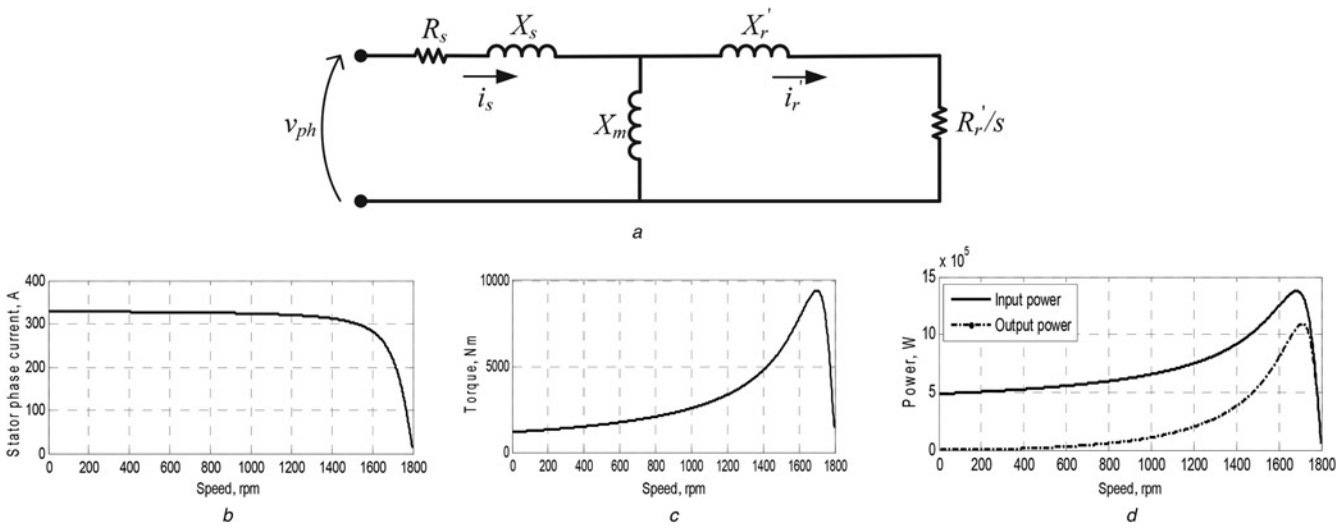

Fig. 4 *Five-phase modular machine characteristics*
a Equivalent per-phase circuit
b Current-speed characteristic
c Torque-speed characteristic
d Power-speed characteristic

If a 5 kHz switching frequency is used, a 3 mH inductor is a proper selection.

On the other hand, if the desired output voltage ripple is 3.5%, the voltage ripple is 312 V, the relation between capacitor voltage ripple and converter capacitance is given by (5)

$$\Delta v_{\mathrm{C}} = \frac{D_{\max}\hat{I}_{\mathrm{ph}}}{C_{\mathrm{i}} f_{\mathrm{s}}} = \frac{0.78\ (70\sqrt{2})}{C_{\mathrm{i}} f_{\mathrm{s}}} \tag{5}$$

For a 5 kHz switching frequency, a 50 µF capacitor is needed.

4.2 Steady-state analysis

Since 60 Hz sinusoidal voltages are fed from the five-phase boost-inverter to the modular machine terminals, a steady-state analysis has been carried out using the machine's per-phase equivalent circuit shown in Fig. 4*a*. The speed is changed from zero to no-load speed (1800 rpm) to calculate the corresponding current, torque and power based on the machine per-phase equivalent circuit. The machine characteristics are shown in Figs. *b–d*. Based on Fig. 4*d*, the efficiency of the machine is 92% at full-load (the rotational losses are neglected).

4.3 Simulation

A MATLAB/SIMULINK model has been built to represent the performance of the proposed system during transients as well as steady-state periods. First, the machine is started at no-load, then the full-load torque is applied at $t = 0.5$ s, the simulation results are shown in Fig. 5. Fig.5*a* shows the voltages and currents of the presented system. It is obvious that the motor phase voltage fed from the boost-inverter is sinusoidal (i.e. the need for filters is eliminated). As a result, the full-load phase currents are also

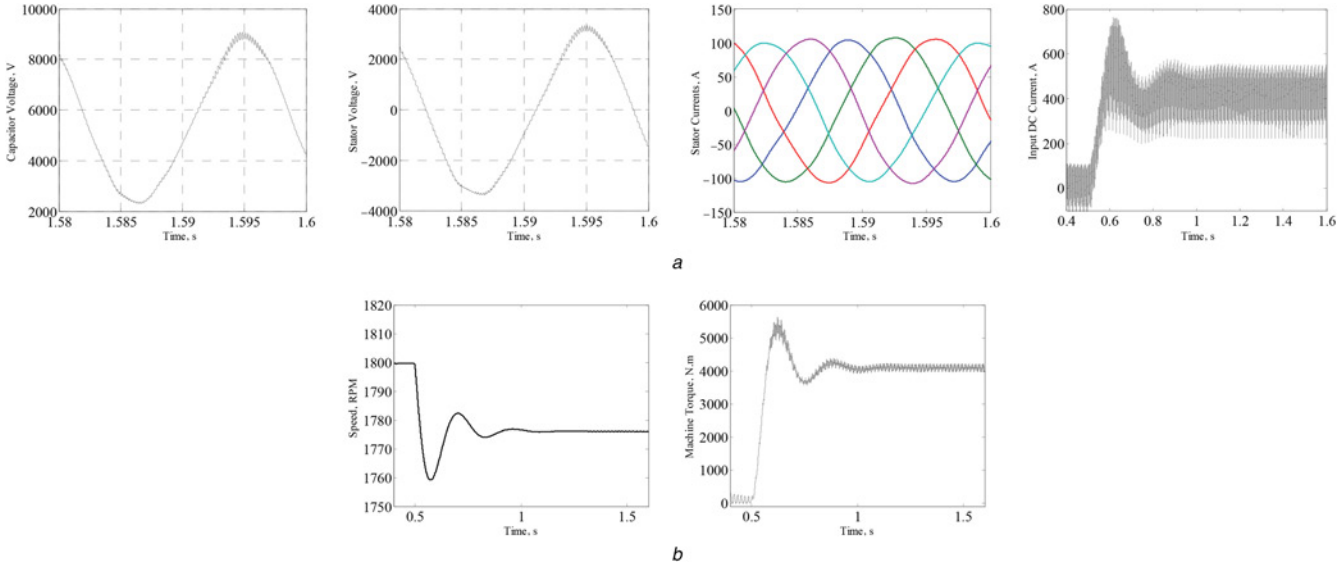

Fig. 5 *Simulation results*
a Electrical variables
b Mechanical variables

doi: 10.1049/joe.2014.0148

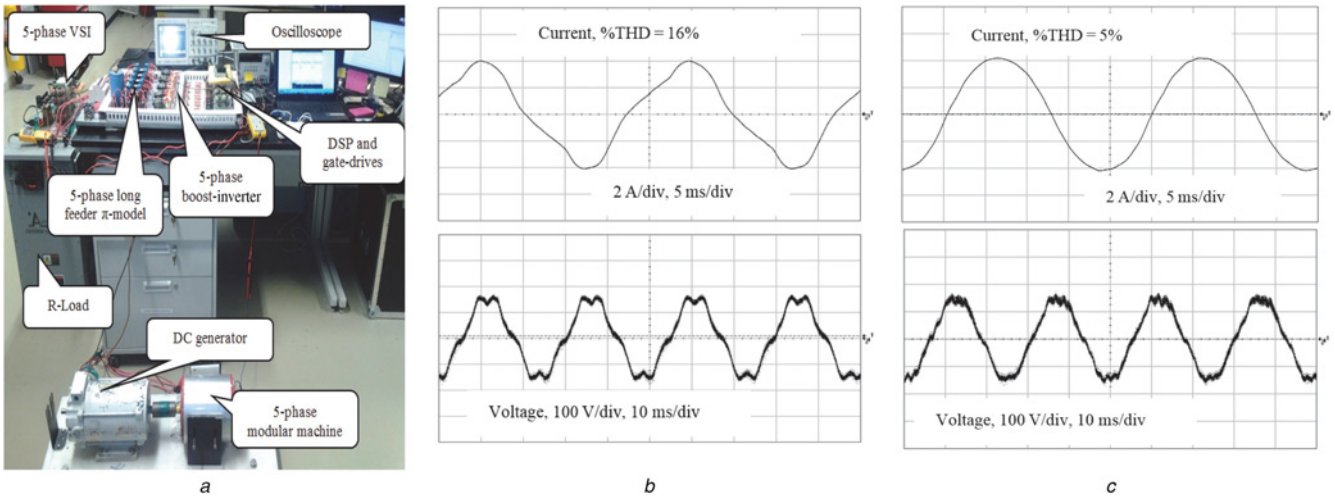

Fig. 6 *Experimental work*
a Experimental setup
b No load stator phase current/voltage
c Full-load Stator phase current/voltage

sinusoidal. In the presented case, the DC input current has a mean of 405 A at full-load. In this simulation, the circuit is fed from a constant DC voltage. Practically, the input current ripples can be significantly reduced with proper DC-link capacitor design. Fig. 5*b* shows the motor speed and torque during no-load as well as full-load conditions.

5 Experimental setup

A small-scale experimental prototype of the proposed system has been built for experimental validation. This is as shown in Fig. 6*a*. A 1 Hp five-phase modular induction machine and boost-inverter are built with the parameters given in Table 2. The machine phase voltage is 110 V rms at 40 Hz. The machine is fed from a five-phase boost-inverter operating at a 5 kHz switching frequency with a 150 V DC supply. The machine is coupled to a PM DC-generator of the same power rating, which acts as a mechanical load. The output power of the generator is measured and added to its losses to estimate the induction machine output mechanical power. A conventional π-network model for each phase with parameters given by Table 2 is implemented to emulate the feeder. The conventional *V*/*f* control is used to control the machine speed. A Texas Instruments TMS320F28335 digital signal processor is used to carry out the control algorithm.

Table 2 Parameters of experimental prototype

	Parameters	Values
five-phase modular machine	rated phase voltage, V, rms	110
	rated phase current, A, rms	3.1
	rated power, Hp	1
	rated frequency, Hz	40
	number of poles	4
	R_s, Ω	8.7
	R_r, Ω	3
	L_s, mH	15.7
	L_r, mH	15.7
	L_m, mH	172
feeder	L_f, mH/km	1.0
	R_f, Ω/km	0.3
	C_f, μF/km	1.0
	feeder length, km	1.0
five-phase boost-inverter	L_i, mH	1.0
	R_i, Ω	0.1
	C_i, μF	30
	V_{dco}, V	310
	V_{aco}, V	160
	f_s, kHz	5
	f, Hz	40

6 Experimental results

This section presents a summary of the main experimental results conducted on the prototype. First, the waveforms of different variables are illustrated under different operating conditions. Next, the machine characteristic curves are presented.

Figs. 6*b* and *c* show the stator phase current/voltage waveforms at no-load as well as full-load conditions, respectively, with inverter rms reference voltage set to (110 V, 40 Hz) using the fundamental sequence. It is noted that the no-load current suffers a high third harmonic component which decreases significantly as the machine is loaded. This third harmonic mainly appears because of core saturation of the prototype machine. However, this problem becomes negligible when the machine is loaded because the internally induced electromotive force (EMF) decreases because of the relatively high stator drop caused by the high stator impedance of the prototype machine. This is common in low-power rating induction machines. As the internally induced EMF decreases with loading, the machine flux decreases, and the magnitude of the third harmonic component significantly decreases. The saturation problem during no-load causes a distortion in the motor terminal phase voltage, as shown in Fig. 6*c*.

Fig. 7 shows the five-phase inverter output currents, the SE line-voltage, the RE line-voltage, the boost-inverter capacitor voltage and the DC input current at full-load condition.

The effect of a sudden change in reference speed at no-load is shown in Fig. 8*a*. It is assumed that the reference frequency is changed from 10 to 40 Hz and the voltage is changed accordingly to maintain a constant *V*/*f* ratio. Another case is shown in Fig. 8*b*, where the machine is suddenly loaded.

It has to be noted that the maximum efficiency of the prototype is relatively low mainly because of the high-power loss in the stator resistance, which is an expected characteristic in low-rating machines. For high-power machines the total machine loss is much smaller, as given by the case study in Section 4.

doi: 10.1049/joe.2014.0148

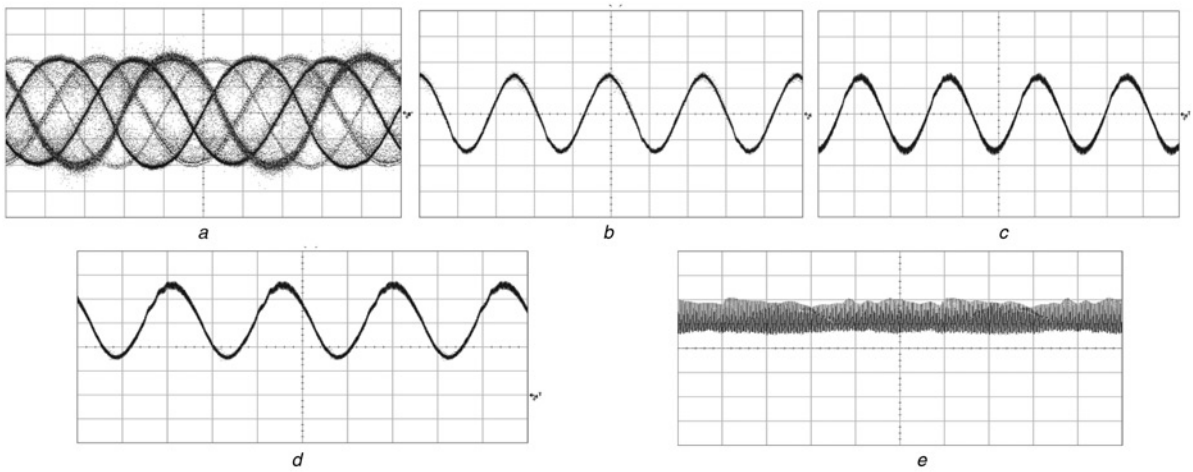

Fig. 7 *Different results of the prototype at full-load conditions*
a Inverter output five-phase currents (2 A/div, 5 ms/div)
b SE line voltage (200 V/div, 10 ms/div)
c RE line voltage (200 V/div, 10 ms/div)
d Boost-inverter capacitor voltage (100 V/div, 10 ms/div)
e Input DC current (10 A/div, 5 ms/div)

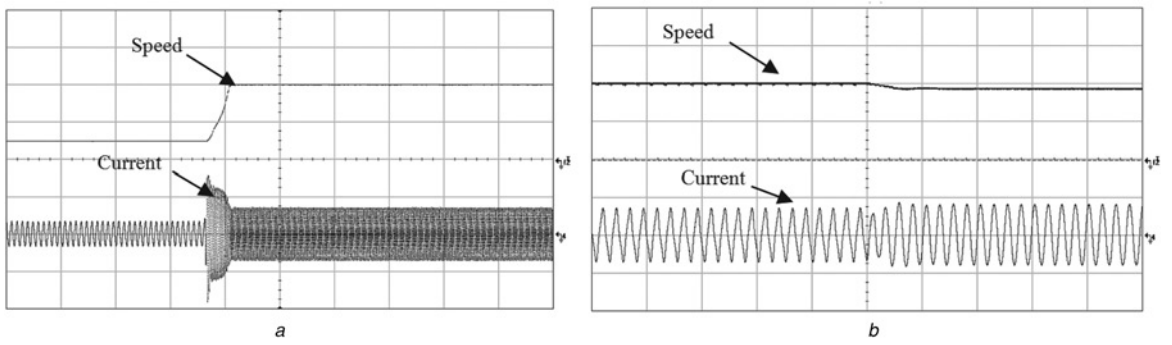

Fig. 8 *Transient current and speed response for a sudden change in the speed*
a From 10 to 40 Hz at no-load (600 rpm/div, 5 A/div, 1 s/div)
b Sudden loading (600 rpm/div, 5 A/div, 0.1 s/div)

7 Conclusion

This paper proposes a new VFD-ESP system which provides potential, economical and technical advantages over the current state-of-the-art. The proposed system can potentially reduce manufacturing cost/time through automated winding, provides transform-less operation and suppresses both differential-mode and common-mode voltages. The system consists of a five-phase modular induction machine at the end of a long feeder fed by a five-phase boost-inverter. The reflected wave phenomenon associated with long feeders is inherently mitigated because of the direct sinusoidal output of the proposed boost-inverter. Hence, the required filter in conventional VSI-based VFD-ESP systems is dispensed with. The additional degrees of freedom offered by the five-phase system add to system features and increase its fault tolerant capability. Additionally, the multiphase machines are generally advantageous with their lower torque ripples and space harmonics, hence, improved drive performance. The performance of the proposed system has been evaluated using an experimental prototype system.

The efficiency of the prototype machine used in this paper is low because of the high stator copper loss; this is not the case with the high-power rated modular machines as shown in the high-power motor design case study. The availability of the boosting function in the boost-inverter makes it possible to use it directly in high-power ESP systems without using a transformer to step up the voltage or install filters.

8 Acknowledgments

This publication was made possible by NPRP grant (NPRP 4-250-2-080) from the Qatar National Research Fund (a member of Qatar Foundation). The statements made herein are solely the responsibility of the authors.

9 References

[1] Al-Haiki Z., Shaikh-Nasser A.: 'Power transmission to distant offshore facilities', *IEEE Trans. Ind. Appl.*, 2011, **47**, pp. 1180–1183
[2] Liang X., Ilochonwu O.: 'Induction motor starting in practical industrial applications', *IEEE Trans. Ind. Appl.*, 2011, **47**, pp. 271–280
[3] Liang X., Faried S., Ilochonwu O.: 'Subsea cable applications in electrical submersible pump systems', *IEEE Trans. Ind. Appl.*, 2010, **46**, pp. 575–583
[4] Liang X., Ilochonwu O., Adedun R.: 'Dynamic response of variable frequency drives in electrical submersible pump systems'. IEEE Industrial and Commercial Power Systems Technical Conf. (I&CPS), 2012, pp. 1–11

[5] Verma V., Singh B., Chandra A., Al-Haddad K.: 'Power conditioner for variable-frequency drives in offshore oil fields', *IEEE Trans. Ind. Appl.*, 2010, **46**, pp. 731–739
[6] Jankowski T.A., Prenger F.C., Hill D.D., *ET AL.*: 'Development and validation of a thermal model for electric induction motors', *IEEE Trans. Ind. Electron.*, 2010, **57**, pp. 4043–4054
[7] Abdel-Khalik A.S., Ahmed S.: 'Performance evaluation of a five-phase modular winding induction machine', *IEEE Trans. Ind. Electron.*, 2012, **59**, pp. 2654–2669
[8] EL-Rafaie A.M., Shah M.R.: 'Comparison of induction machine performance with distributed and fractional-slot concentrated windings'. Conf. Record IEEE IAS Annual Meeting, 2008, pp. 1–8
[9] Levi E.: 'Multiphase electric machines for variable-speed applications', *IEEE Trans. Ind. Electron.*, 2008, **55**, pp. 1893–1909
[10] Abdelsalam A.K., Masoud M.I., Finney S.J., Williams B.W.: 'Vector control PWM-VSI induction motor drive with a long motor feeder: performance analysis of line filter networks', *IET Electr. Power Appl.*, 2011, **5**, pp. 443–456
[11] Wang L., Ngai-Man Ho C., Canales F., Jatskevichm J.: 'High-frequency modeling of the long-cable-fed induction motor drive system using TLM approach for predicting overvoltage transient', *IEEE Trans. Power Electron.*, 2010, **25**, pp. 2653–2664
[12] Tallam R., Skibinski G., Shudarek T., Lukaszewski R.: 'Integrated differential-model and common-model filter to mitigate the effects of long motor leads on AC drives', *IEEE Trans. Ind. Appl.*, 2011, **47**, pp. 2075–2083
[13] Hava A., Ün E.: 'A high-performance PWM algorithm for common-mode voltage reduction in three-phase voltage source inverters', *IEEE Trans. Power Electron.*, 2011, **26**, pp. 1998–2008
[14] von Jouanne A., Rendusara D.A., Enjeti P.N., Gray J.W.: 'Filtering techniques to minimize the effect of long motor leads on PWM inverter-fed AC motor drive systems', *IEEE Trans. Ind. Appl.*, 1996, **32**, pp. 919–926
[15] von Jouanne A., Enjeti P.N.: 'Design considerations for an inverter output filter to mitigate the effects of long motor leads in ASD applications', *IEEE Trans. Ind. Appl.*, 1997, **33**, pp. 1138–1145
[16] Rendusara D.A., Enjeti P.N.: 'An improved inverter output filter configuration reduces common and differential modes DV/DT at the motor terminals in PWM drive systems', *IEEE Trans. Power Electron.*, 1998, **13**, pp. 1135–1143
[17] Habetler T.G., Naik R., Nondahl T.A.: 'Design and implementation of an inverter output LC filter used for DV/DT reduction', *IEEE Trans. Power Electron.*, 2002, **17**, pp. 327–331
[18] Chen X., Xu D., Liu F., Zhang J.: 'A novel inverter-output passive filter for reducing both differential- and common-mode dv/d*t* at the motor terminals in PWM drive systems', *IEEE Trans. Ind. Electron.*, 2007, **54**, pp. 419–426
[19] Moreira A.F., Santos P.M., Lipo T.A., Venkataramanan G.: 'Filter networks for long cable drives and their influence on motor voltage distribution and common-mode currents', *IEEE Trans. Ind. Electron.*, 2005, **52**, pp. 515–522
[20] C'aceres R.O., Barbi I.: 'A boost DC–AC converter: analysis, design, and experimentation', *IEEE Trans. Power Electron.*, 1999, **14**, pp. 134–141
[21] Sanchis P., Ursæa A., Gubía E., Marroyo L.: 'Boost DC–AC inverter: a new control strategy', *IEEE Trans. Power Electron.*, 2005, **20**, pp. 343–353
[22] Cecati C., Dell'Aquila A., Liserre M.: 'A novel three-phase single-stage distributed power inverter', *IEEE Trans. Power Electron.*, 2004, **19**, pp. 1226–1233

10 Appendix

Boost converter design

(1) *Inductor selection:* During the instant of inductor current peak (i.e. maximum duty cycle), the power balance equation for the boost converter circuit is given by (6)

$$P_{\mathrm{i}} = P_{\mathrm{L\ Loss}} + P_{\mathrm{o}} \tag{6}$$

where P_{i} is the input DC power at this instant $= I_{\mathrm{L\ max}} V_{\mathrm{dc}}$, $P_{\mathrm{L\ Loss}}$ is the power loss in the inductor $= R_{\mathrm{i}} I^2_{\mathrm{L\ max}}$, P_{o} is the output power at this instant $= \hat{v}_{\mathrm{c}} \hat{I}_{\mathrm{Ph}}$. That is

$$(-V_{\mathrm{dc}} I_{\mathrm{L\ max}} + R_{\mathrm{i}} I^2_{\mathrm{L\ max}} + \hat{v}_{\mathrm{c}} \hat{I}_{\mathrm{Ph}} = 0) \tag{7}$$

By solving this second-order algebraic equation, the inductor current peak is given by (8)

$$I_{\mathrm{L\ max}} = \frac{V_{\mathrm{dc}} - \sqrt{V^2_{\mathrm{dc}} - 4R_{\mathrm{i}} \hat{v}_{\mathrm{c}} \hat{I}_{\mathrm{Ph}}}}{2R_{\mathrm{i}}} \tag{8}$$

From DC–DC boost converter basics, the expression for inductor current ripple is given by (9)

$$\Delta I_{\mathrm{L}} = \frac{(V_{\mathrm{dc}} - I_{\mathrm{L\ max}}\, R_{\mathrm{i}}) D_{\mathrm{max}}}{L_{\mathrm{i}} f_{\mathrm{s}}} \tag{9}$$

where

$$D_{\mathrm{max}} = 1 - \frac{V_{\mathrm{dc}}}{\hat{v}_{\mathrm{C}}} \tag{10}$$

For a desired switching frequency and desired level of inductor current ripples, a suitable inductor can be selected. Practically, the inductor current ripple is selected to be 20% of the inductor current peak [20].

(2) *Capacitor selection:* From DC–DC boost converter basics, the output voltage ripple is given by (11)

$$\Delta v_{\mathrm{C}} = \frac{D_{\mathrm{max}} \hat{I}_{\mathrm{ph}}}{C_{\mathrm{i}} f_{\mathrm{s}}} \tag{11}$$

For a desired switching frequency and desired level of output voltage ripple, a suitable capacitor can be selected. Practically the output voltage ripple is selected to be lower than 5% of $\hat{v}_{\mathrm{c}}$ [20].